Limits on information transduction through amplitude and frequency regulation of transcription factor activity

Anders S Hansen, Erin K O'Shea

DOI: http://dx.doi.org/10.7554/eLife.06559

Cite as: eLife 2015;10.7554/eLife.06559

Received: 19 January 2015
Accepted: 17 May 2015
Published: 18 May 2015

TITLE

Limits on Information Transduction through Amplitude and Frequency Regulation of Transcription Factor Activity

AUTHOR NAMES & AFFILIATIONS

Anders S. Hansen[1,2,3] and Erin K. O'Shea[1,2,3,4,*]

[1]Department of Chemistry and Chemical Biology, Harvard University, 12 Oxford Street, Cambridge, MA 02138, USA

[2]Howard Hughes Medical Institute

[3]Faculty of Arts and Sciences Center for Systems Biology

[4]Department of Molecular and Cellular Biology

Harvard University, Northwest Laboratory, 52 Oxford Street, Cambridge, MA 02138, USA

CONTACT

*Correspondence: erin_oshea@harvard.edu

ABSTRACT

Signaling pathways often transmit multiple signals through a single shared transcription factor (TF) and encode signal information by differentially regulating TF dynamics. However, signal information will be lost unless it can be reliably decoded by downstream genes. To understand the limits on dynamic information transduction, we apply information theory to quantify how much gene expression information the yeast TF Msn2 can transduce to target genes in the amplitude or frequency of its activation dynamics. We find that although the amount of information transmitted by Msn2 to single target genes is limited, information transduction can be increased by modulating promoter *cis*-elements or by integrating information from multiple genes. By correcting for extrinsic noise, we estimate an upper bound on information transduction. Overall, we find that information transduction through amplitude and frequency regulation of Msn2 is limited to error-free transduction of signal identity, but not signal intensity information.

INTRODUCTION

Cellular signaling pathways often exhibit a bowtie topology (Csete and Doyle, 2004): multiple distinct signal inputs converge on a single master regulator, typically a transcription factor (TF), which then controls the expression of partially overlapping sets of downstream target genes. This raises two general questions: first, how can the cell encode information about different signals in the activity of a single master TF? Second, can this information be decoded by target genes to elicit a specific output for each input?

One way the cell can encode signal information is by regulating the activation dynamics of a single master TF (Figure 1A). For example, p53, a tumor suppressor TF, exhibits an intensity-dependent number of nuclear pulses in response to γ-radiation, but a sustained pulse of nuclear localization with intensity-dependent amplitude during UV-radiation (Batchelor et al., 2011; Lahav et al., 2004). Akin to p53, the yeast multi-stress response TF Msn2 exhibits short pulses of nuclear localization with intensity-dependent frequency under glucose limitation, but sustained nuclear localization with intensity-dependent amplitude under oxidative stress (Hao et al., 2013; Hao and O'Shea, 2012; Jacquet et al., 2003; Petrenko et al., 2013). Thus, p53 and Msn2 dynamics encode both signal identity and signal intensity. Beyond p53 and Msn2, amplitude- or frequency encoding of signal identity and intensity information is conserved throughout eukaryotic signaling pathways (see also (Albeck et al., 2013; Aoki et al., 2013; Berridge et al., 2000; Cai et al., 2008; Dalal et al., 2014; Harima et al., 2014; Imayoshi et al., 2013; Warmflash et al., 2012; Werner et al., 2005)). Such encoding of signal identity and intensity information in TF activation dynamics has led to the hypothesis that TF target genes can reliably decode this dynamical information to elicit distinct gene expression programs with fine-tuned expression levels (Figure 1A) (Behar et al., 2007; Behar and Hoffmann, 2010; de Ronde and ten Wolde, 2014; Hansen and O'Shea, 2013; Levine et al., 2013; Purvis and Lahav, 2013; Yosef and Regev, 2011).

However, non-genetic cell-to-cell variability (noise) in gene expression limits the fidelity with which information can be decoded by TF target genes (Coulon et al., 2013; Sanchez and Golding, 2013). This is important because the capacity of any signaling pathway for information transduction is limited by the capacity of its weakest node or bottleneck (Cover and Thomas, 2006). Thus, even though information can reliably be encoded in TF activation dynamics (Selimkhanov et al., 2014), this information will be lost unless genes can reliably decode it. We therefore focus on the response of single genes and ask: can cells reliably transmit both signal identity and intensity information in the amplitude and frequency of TFs to target genes in the presence of biochemical noise? In other

words, what are the limits on amplitude- and frequency-mediated information transduction? We investigate this by applying tools from information theory to quantify how much of the information (in bits) encoded in the amplitude and frequency of a TF can be transmitted through gene promoters to fine-tune the gene expression level.

Originally developed by Claude Shannon for communication systems (Shannon, 1948), information theory has recently been applied to cell signaling (reviewed in (Bowsher and Swain, 2014; Levchenko and Nemenman, 2014; Mc Mahon et al., 2014; Nemenman, 2012; Rhee et al., 2012; Tkacik and Walczak, 2011; Waltermann and Klipp, 2011)). Mutual information quantifies how much information an output can carry about an input across a noisy channel (Figure 1B). Mathematically, information is quantified in bits: to resolve two different signal intensities without error requires at least 1 bit of information, to resolve four different signal intensities without error requires at least 2 bit of information and so forth. However, 1 bit of information does not guarantee that two intensities can be distinguished without error. Similarly, 1 bit may allow multiple intensities to be distinguished, albeit with some associated error (Bowsher and Swain, 2014). As an example of how information theory can be applied, consider a dose-response relationship (Figure 1B). A graded population-level dose-response can belie the complexity of the single-cell response (Ferrell and Machleder, 1998). For example, if different TF amplitudes or frequencies lead to distinguishable gene expression outputs (points a, b, c and d), signal intensity information is accurately transmitted and the cell can fine-tune the expression of stress genes to the stress intensity like a "rheostat" (Figure 1C, rheostat model). However, biochemical noise can degrade signal information: if gene expression outputs are no longer resolvable, the cell can no longer fine-tune the expression level of stress genes to stress intensity (Figure 1C, noisy switch model). In the noisy switch model, the cell can distinguish no stimulus (point a, OFF) from maximal stimulus (point d, ON) – but intermediate stimuli (points b and c) cannot reliably be distinguished based on the gene expression output and signal intensity information has been lost (Figure 1C). Information theory provides a framework for capturing and quantifying these differences. Thus, we can distinguish these two models by measuring information transduction by promoters: the noisy switch model requires ~1 bit, whereas the rheostat model requires substantially higher mutual information.

Previous applications of information theory have been theoretical (Bowsher and Swain, 2012; de Ronde et al., 2011; Lestas et al., 2010; Rieckh and Tkacik, 2014; Tostevin and ten Wolde, 2009; Ziv et al., 2007) or have focused on upstream signaling and development (Cheong et al., 2011; Dubuis et al., 2013; Gregor et al., 2007; Mehta et al., 2009; Selimkhanov et al., 2014; Skerker et al.,

2008; Tkacik et al., 2008; Tkacik et al., 2009; Tostevin et al., 2007; Uda et al., 2013; Voliotis et al., 2014). However, despite gene expression being the final bottleneck in cell signaling, gene expression has received little attention (Uda et al., 2013). Estimating an upper limit on the information transduction capacity of a gene has not previously been possible due to extrinsic noise: even when studying genetically identical single cells, the cells can exhibit non-genetic differences, e.g. in cell cycle phase or variability in TF concentration, which means the measured mutual information will be an underestimate (Elowitz et al., 2002; Toettcher et al., 2013). Here we overcome this limitation through a combined experimental and theoretical approach that corrects for extrinsic noise and allows us to estimate an upper limit on the information transduction capacity of individual Msn2 target genes.

We combine high-throughput microfluidics to control the amplitude and frequency of Msn2 nuclear translocation with information theory to determine the information transduction capacity of Msn2 target genes. We find that Msn2 target genes can transduce just over 1 bit of information, consistent with the "noisy switch model". Although individual Msn2 target genes can only transduce little information, we illustrate how the cell can improve information transduction capacity by modulating promoter *cis*-elements, by integrating the response of more than one gene, or by having multiple copies of the same gene. We show that more information can be transduced through amplitude than through frequency modulation of Msn2 activation dynamics. Nevertheless, while previous studies have shown that significant amounts of information can be encoded in TF activation dynamics (Selimkhanov et al., 2014), we find that noise in the decoding step severely limits information transduction. Specifically, our results indicate that information about signal identity, but not signal intensity, can be transmitted nearly without error in the amplitude and frequency of Msn2 and decoded by Msn2-responsive promoters.

RESULTS

Quantifying information transduction using information theory

Information theory quantifies information transduction across a channel between a signal and a response (Cover and Thomas, 2006; Shannon, 1948). If a channel is noisy, a given signal input will give rise to a distribution of response outputs. This represents a loss of information since the signal input can no longer reliably be learned from observing the response output (Figure 1B-C). A "black-box"-framework, information theory was originally developed for telecommunication channels, but it can also be applied to other "channels" such as gene promoters or cell signaling pathways provided that the signal input (here amplitude or frequency of Msn2 activation) can be precisely controlled and the response output distribution precisely measured (here single-cell gene expression). Mutual information, $MI(R;S)$, measured in bits, quantifies the amount of information about the signal input (S) that can be obtained by observing the response output (R) and, given discretized data, is defined as:

$$MI(R;S) = \sum_{i,j} p(R_i, S_j) \log_2 \left(\frac{p(R_i, S_j)}{p(R_{ij}) p(S_j)} \right) \quad \text{(equation 1)}$$

The response distribution, $p(R)$, is the experimentally measured distribution of gene expression output. The signal distribution, $p(S)$, is the relative probability of each Msn2 amplitude or frequency. Since $MI(R;S)$ depends on $p(S)$ and since $p(S)$, e.g. how often a cell might be exposed to a particular intensity of oxidative stress, is unknowable, hereafter we consider the maximal mutual information, I ($I(R;S) = \max_{p(S)} [MI(R;S)]$) which is the maximal amount of information that can be transduced through a "promoter channel". I can be thought of as a channel capacity, though a gene promoter is effectively a "single-use" channel and I therefore has units of bits, whereas messages are sent repeatedly through a Shannon channel and, accordingly, the channel capacity has units of bits/s ((Bowsher and Swain, 2014); a detailed discussion is given in Supplementary File 2).

Natural Msn2 target genes have low information transduction capacities

To measure how much information Msn2 target genes can transduce, we took advantage of a pharmacological method for controlling Msn2 nuclear localization using a small molecule, 1-NM-PP1, (Bishop et al., 2000; Hao and O'Shea, 2012; Zaman et al., 2009) and high-throughput microfluidics coupled to quantitative time-lapse microscopy (Hansen et al., 2015; Hansen and O'Shea, 2013). With this setup (Figure 2 – figure supplement 1A; Video 1), we can control and

measure the amplitude and frequency of activation of an Msn2-mCherry fusion protein over time and generate single-cell traces that mimic the natural Msn2 dynamics under oxidative stress (a sustained nuclear pulse with signal intensity–dependent amplitude; Figure 2A) and glucose limitation (short pulses with signal intensity–dependent frequency; Figure 2B) (Hao and O'Shea, 2012; Petrenko et al., 2013). To measure stress-relevant gene expression, we use CFP/YFP fluorescent reporters and focus on two specific Msn2 target genes: *HXK1*, which is induced under glucose limitation (Herrero et al., 1995) and *SIP18*, which is induced in response to oxidative stress (Rodriguez-Porrata et al., 2012). Using this setup, we have previously shown that, at the population level, individual genes differentially decode Msn2 dynamics (Hansen and O'Shea, 2013; Hao and O'Shea, 2012): oscillatory Msn2 activation induces gene class B (e.g. *HXK1*) without inducing gene class A (e.g. *SIP18*), whereas sustained Msn2 activation preferentially induces gene class A (Figure 1A). Thus, this represents an ideal setup for studying promoter decoding of Msn2 dynamics in single cells, which enables us to quantify information transduction.

To measure information transduction through the *HXK1* and *SIP18* promoters with respect to amplitude modulation (I_{AM}), we exposed thousands of cells to increasing amplitudes of a 70 min Msn2 pulse to mimic oxidative stress, measured the single-cell distribution of responses for each amplitude with minimal measurement noise (Figure 2 – figure supplement 2), and determined the population-averaged dose-response (Figure 2A; all raw single-cell data is available online as Supplementary File 1 and in (Hansen and O'Shea, 2015); see also Figure 2 – figure supplement 1B). We quantify gene expression as the maximal YFP concentration after the YFP time-trace has reached a plateau (Materials and Methods). Surprisingly, for both *HXK1* and *SIP18,* I_{AM} was 1.2-1.3 bits – enough to distinguish ON from OFF without error (the 'no Msn2 input' and the 'brown' distributions are clearly distinguishable; Figure 2A), but with limited ability to distinguish signal intensities. One way to think about this result is to ask, given the *HXK1* YFP expression output, how much information does that provide about the input amplitude? For example, considering the *HXK1* AM histograms in Figure 2A, for most YFP outputs the cell can exclude the 'no Msn2 input' condition, but appears to be unable to discern which of the other amplitudes it was exposed to without a high error rate. Consequently, *HXK1* and *SIP18* can distinguish no stress from high oxidative stress (high Msn2 amplitude) without error, but cannot accurately transmit information about stress intensity.

Next, we measured information transduction of *HXK1* and *SIP18* with respect to frequency modulation (I_{FM}) using 5-min Msn2 pulses at frequencies similar to those observed under glucose

limitation (Figure 2B). Even though *HXK1* is physiologically induced during Msn2 pulsing, I_{FM} was only 1.11 bits – again enough for distinguishing ON from OFF essentially without error like a "noisy switch", but insufficient to accurately fine-tune the *HXK1* expression level to each Msn2 frequency like a "rheostat". *SIP18*, required only under oxidative stress, largely filters out Msn2 pulsing and therefore has a negligible I_{FM}.

The promoter information transduction capacity is tunable and can be increased for natural Msn2 target genes

It is generally assumed that gene expression levels are fine-tuned (de Nadal et al., 2011), but the very low I_{AM} and I_{FM} of *HXK1* and *SIP18* are incompatible with this idea. One possibility is that mutual information for promoters is biophysically constrained to ~1.0-1.3 bit, but another possibility is that *HXK1* and *SIP18* are not optimized for AM- and FM-mediated information transduction. To investigate this and explore the relationship between promoter *cis*-elements and information transduction we focused on *SIP18*, which has the lowest *I* and suffers from high gene expression noise (Figure 2 – figure supplement 1D), and asked if altering promoter architecture could improve information transduction. We removed the two functional Msn2 binding sites in the *SIP18* promoter and added three and four new binding sites in the nucleosome-free region closer to the transcription start site (promoter architecture maps are shown in Figure 2 – figure supplement 1C) to generate *pSIP18* mut A and *pSIP18* mut B, which differ from the wild-type *SIP18* promoter by 14 and 18 nucleotides, respectively. We then repeated the experiments for mut A and mut B to measure their I_{AM} and I_{FM}.

With respect to amplitude modulation (AM), both mutants had significantly higher I_{AM} of 1.42 bits (mut A) and 1.55 bits (mut B) (Figure 2C). We attribute this increase to a combination of three factors: a more linear dose-response, a higher dynamic range and significantly lower gene expression noise (Figure 2 – figure supplement 1D).

The wild-type *SIP18* promoter filters out oscillatory input and therefore has a negligible I_{FM}. In contrast, with respect to frequency modulation (FM) mut A shows a slightly higher I_{FM} of 0.88 bits and mut B a significantly higher I_{FM} of 1.39 bits (Figure 2D). Notably, although *HXK1* presumably evolved to decode Msn2 pulsing, as is observed under glucose limitation, mut B now shows a higher I_{FM} than even *HXK1*. Although *I* could be different for natural Msn2 dynamics (Hao and O'Shea, 2012), these results show that for the AM and FM signals studied here, natural Msn2 target genes are not optimized for information transduction and do not have their maximal *I*

even though promoters with higher $I_{AM/FM}$ are only a few mutations away. Furthermore, I_{AM} exceeds I_{FM} for all four promoters, which shows that, at least in these four cases, transmitting gene expression information in the amplitude of TF activation dynamics is more reliable than transmitting it in the frequency. Thus, the promoter information transduction capacity is tunable in *cis*: by modulating Msn2 binding sites, we can control both how a promoter decodes Msn2 dynamics and how much information it can transmit.

Estimating the intrinsic information transduction capacity of promoters

Natural Msn2 target promoters appear to have $I \leq 1.3$ bits. Thus, we observe high information loss during gene expression. Information loss comes from two sources: gene-intrinsic and gene-extrinsic noise (Elowitz et al., 2002). Intrinsic noise originates from the inherently stochastic nature of biochemical reactions, such as stochastic binding of Msn2 at individual promoters. Information loss due to intrinsic noise is therefore unavoidable for the cell. Extrinsic noise comes from the intracellular environment, which may differ between cells in a population. Even though we consider genetically identical cells grown in a microfluidic chemostat, the cell population could exhibit non-genetic differences in cell-cycle phase and Msn2 abundance or dynamics etc. This could cause the dose-response to be different between single cells (Figure 3A), as was observed in a recent study on Ras/ERK signaling (Toettcher et al., 2013). For example, a cell with a higher-than-average Msn2 abundance might show higher gene expression. When we carefully quantify Msn2-mCherry dynamics, we observe loss of information between the microfluidic 1-NM-PP1 input and nuclear Msn2 due to variability in Msn2 abundance between cells (Figure 3 – figure supplement 1). Likewise, the cell cycle is a major source of extrinsic gene expression noise (Zopf et al., 2013). Therefore, measuring mutual information in a cell population subject to extrinsic noise, as we did in Figure 2, underestimates the intrinsic information transduction capacity of a promoter.

Although it is in principle possible to correct for cell cycle phase, Msn2 abundance and other gene-extrinsic factors individually, it is impossible to correct for all factors. To overcome this limitation and estimate the intrinsic I (I_{int}), we developed a method based on the dual-reporter approach (Elowitz et al., 2002; Hilfinger and Paulsson, 2011; Swain et al., 2002). By having two gene expression reporters in diploid cells on homologous chromosomes that differ only by their color (CFP and YFP) but share the same intracellular environment, the extent to which they co-vary in the same cell allows us to infer how much gene-extrinsic factors such as cell-cycle phase and Msn2 variability etc. contribute altogether (extrinsic noise), without having to specify each factor. Or

phrased differently, if the dose-response is shifted in a cell, both the CFP and YFP reporter will be affected in a correlated manner and their covariance allows us to quantify this (Figure 3A). Therefore, we developed an algorithm that uses the CFP/YFP covariance to estimate what the intrinsic *I* (I_{int}) would have been in the absence of extrinsic noise. Briefly, our algorithm takes the following steps (Figure 3B): First, the raw YFP histogram is fitted to a gamma distribution ($\text{YFP} \sim \Gamma(a,b)$). Second, the extrinsic component (covariance) of the total variance is determined ($\sigma^2_{\text{ext}} = \langle \text{CFP} \cdot \text{YFP} \rangle - \langle \text{CFP} \rangle \langle \text{YFP} \rangle$). Third, keeping the mean constant, a new gamma distribution without the extrinsic component is inferred ($\text{YFP} \sim \Gamma(a_{\text{int}}, b_{\text{int}})$). Fourth, this is repeated for each Msn2 input (e.g. amplitude or frequency). Finally, this inferred dataset is discretized and then used to estimate I_{int} (Figure 3B; see Supplementary File 2 for a detailed discussion of the algorithm). We verified our algorithm *in silico* by systematically simulating five linear and five non-linear gene expression models with and without extrinsic noise and compared the true I_{int} to the algorithm-inferred I_{int}. The algorithm tended to slightly underestimate the true I_{int}, but the mean error was less than 2% and the error was always less than 5% (Supplementary File 2).

Therefore, by using dual-reporter strains we can determine how much of the information loss is extrinsic, apply the algorithm and estimate I_{int} in each case ($I_{\text{AM,int}}$ and $I_{\text{FM,int}}$). We find that filtering out extrinsic noise significantly increases *I* (hatched bars, Figure 3C). Since the cell most likely incorporates some gene-extrinsic factors into a decision, but most likely does not incorporate all gene-extrinsic factors, we interpret I_{raw} and I_{int} as a lower and upper bound, respectively, on the true *I*. Thus, our approach allows us to estimate an upper bound, I_{int}, on a promoter's information transduction capacity.

Even after correcting for extrinsic noise, $I_{\text{AM,int}}$ for *HXK1* and *SIP18* only reach ~1.5-1.6 bits (Figure 3C). And $I_{\text{FM,int}}$ for *HXK1* is just 1.36 bits – that is, three ranges of inputs can only be distinguished with some associated error. Thus, even when considering I_{int}, which is the upper limit on the maximal mutual information, neither natural Msn2 target gene can transmit information about stress intensity without some error. That is, consistent with the "noisy switch model", expression of *HXK1* and *SIP18* is not reliably fine-tuned to stress intensity. In contrast, for mut B $I_{\text{FM,int}}$ is 1.55 bits and $I_{\text{AM,int}}$ is ~2 bits (Figure 3C). Thus, mut B almost approaches a range where information about both signal identity and intensity could conceivably be transduced nearly without error like a "rheostat", though the natural Msn2 target genes, *HXK1* and *SIP18*, do not.

Multiple gene copies reduces information loss due to intrinsic noise

Filtering out extrinsic noise substantially increases *I* (Figure 3C). Next, we considered how reducing intrinsic noise might increase *I*. In principle, as the number of gene copies increases, information loss due to intrinsic noise decreases due to simple ensemble averaging and mutual information increases – in the limit of infinite copies, intrinsic noise is zero and all information loss is due to extrinsic noise (Cheong et al., 2011). To test this we generated diploid strains with either one (1x) or two (2x) copies of the *hxk1*::CFP and *sip18*::YFP reporters in the same cell.

We repeated the AM and FM experiments for the 1x and 2x diploids (Figure 4 – figure supplement 1 and 2). Comparing the 1x and 2x diploids (Figure 4A), we see that having two copies of a gene generally improves *I* by ~0.05-0.20 bits. For example, on going from haploid (1x) to diploid (2x), *HXK1* I_{AM} increases from 1.30 to 1.47 bits. Therefore, in terms of information transduction, being diploid confers a small but robust advantage.

Circuits integrating the response of two genes can transduce more information than single gene circuits

So far we have considered information transduction from Msn2 to a single gene. Yet, Msn2 controls the expression of hundreds of genes in response to different stresses (Elfving et al., 2014; Hao and O'Shea, 2012; Huebert et al., 2012), We therefore extend our approach to information transduction from Msn2 to multiple genes. We next asked whether one way the cell might overcome the low *I* of individual genes would be to integrate the response of two or more different genes. To simulate and test this, we used diploid strains with both *hxk1*::CFP and *sip18*::YFP in the same cell, which allows us to measure the joint mutual information, $I(\boldsymbol{R}_1,\boldsymbol{R}_2;\boldsymbol{S})$.

We find that the AM joint mutual information ($I_{AM,joint}$) is significantly higher in both the 1x and 2x cases than the individual I_{AM} of *HXK1* and *SIP18* (Figure 4A). For example, the total joint mutual information ($I_{AM+FM,joint}$; combining both the AM and FM responses) is 1.67 bits and 1.83 bits for the 1x and 2x diploids, respectively (Figure 4A). For example, although *HXK1* and *SIP18* individually can only distinguish ON from OFF without error (Figure 2A), their joint response can distinguish three inputs (no input, FM or AM) nearly without error (Figure 4B).

Thus, these results show that although the information transduction capacities of individual genes may be low, by integrating the response of two different genes the cell can improve information transduction. Therefore, by integrating the response of even more than two genes, the cell could potentially substantially improve the information transduction capacity of a pathway.

DISCUSSION

Here we use information theory to investigate the hypothesis that cells can transduce both signal identity and signal intensity information in the amplitude and frequency of TF activation dynamics to control gene expression. As a conceptual framework, we introduce two extreme models of information transmission (Figure 1C): in the "noisy switch model", the cell only transmits information sufficient to turn ON or OFF particular genes or pathways in response to external signals or stresses, whereas in the "rheostat model" the cell is accurately fine-tuning the expression levels of relevant genes to the intensity of a signal or stress. For a TF responding to multiple stresses, we can extend this framework beyond a single gene. Extending the noisy switch model to two genes, the stress-relevant gene *HXK1* is reliably induced during FM pulsing of Msn2 (as seen under glucose limitation), whereas both *HXK1* and the stress-relevant *SIP18* gene are reliably induced during AM activation of Msn2 (as seen under oxidative stress) (Figure 4B). Therefore, three inputs (no input, FM or AM) can be distinguished essentially without error (Figure 4B). However, given the modest joint information transduction capacities with respect to AM and FM combined ($I_{\mathrm{AM+FM,joint}}$; Figure 4A), the cell cannot fine-tune *HXK1* and *SIP18* expression levels without significant error to the stress intensity. Thus, signal identity information for two distinct stresses can be transduced in the amplitude and frequency of Msn2 essentially without error, but intensity information can only be transduced with high error.

A central result in information theory is that the information transduction capacity of a signaling pathway is limited by and equal to the capacity of its weakest node or bottleneck (see also Supplementary File 2 for a discussion). In other words, once information has been lost, no amount of post-processing can recover it, as is seen in the game of "broken telephone". Therefore, by measuring information transduction of individual Msn2 target genes to be ~1.0-1.3 bits, we can establish that the expression of Msn2 target genes cannot transduce stress signal intensity information without significant error at least for the AM and FM signals studied here – we can draw this conclusion without knowing all the relevant upstream components of the signaling pathway, how they mechanistically interact and how much information they can transmit. Thus, this approach can provide insight into the purpose of a pathway (e.g. noisy switch vs. rheostat) and can readily be applied to other signaling pathways.

Why does information transduction by Msn2 resemble a "noisy switch" rather than a "rheostat"? Or phrased differently, why should the cell not fine-tune the expression level of stress genes to the stress intensity? One possibility is that the stochasticity inherent in the biophysical

process of transcription fundamentally constrains information transduction by a promoter to ~1.0-1.3 bit. However, since the information transduction capacity of *SIP18* can be substantially increased by modulating promoter *cis*-elements (Figure 2 and 3), the low *I* of natural Msn2 target genes is not solely due to inherent biophysical constraints. Another speculative possibility is that variability is selected for: since evolutionary selection works at the population-level, variability in gene expression can create phenotypic diversity within an isogenic population (Balaban et al., 2004; Blake et al., 2006). It is also important to note that under natural stress a network of factors could be activated, whereas here we study the limits on amplitude- and frequency-mediated transduction of gene expression information in the dynamics of a single master TF.

Many biological signaling pathways transmit information through the amplitude or frequency of a shared signaling molecule (Figure 1A) and this has raised the long-standing question: can more information be transmitted through the amplitude or the frequency of a signaling molecule (Li and Goldbeter, 1989; Rapp et al., 1981)? This question has not previously been experimentally addressed for TFs responding to multiple signals in an amplitude- or frequency-dependent manner. We show that more gene expression information can be transduced through the amplitude than through the frequency of Msn2 activation dynamics for all genes studied here (Figure 2 and 3). Although the FM dose-responses tend to be more linear, the AM dose-responses have higher dynamic range and lower noise (Figure 2 and Figure 2 – figure supplement 1D). While we show that gene promoters have higher information transduction capacities for amplitude- than frequency-encoded information (Figure 2 and 3), maximal information transduction can be achieved for TFs that exhibit both amplitude- and frequency-encoding (Figure 4).

The amount of information promoters measured in this study can transmit is limited (Figure 2-4); yet we stress that for many "house-keeping" genes or genes expressed at steady-state information transduction is likely significantly higher, in part due to time-averaging. Indeed, the gene expression response to a transient signal is noisier than a response at steady-state (Hansen and O'Shea, 2013) and inducible genes tend to show higher expression noise (Bar-Even et al., 2006; Newman et al., 2006). One way the cell can improve information transduction is by integrating the response of more than one gene or by having multiple copies of a gene (Figure 4). An example of this is ribosome biogenesis where, by having multiple copies of each gene encoding a subunit and employing elaborate feedback control, the cell can fine-tune its translational capability to its growth and energy status (Lempiainen and Shore, 2009). Another example is morphogen or cytokine secretion: although the amount produced by each single cell might be noisy, the average amount

produced by a large number of cells can be highly precise (Cheong et al., 2011; Gregor et al., 2007). Hence, a number of strategies for increasing information transmission exist.

In conclusion, we have investigated the reliability of transmitting gene expression information in the amplitude and frequency of a TF. We show that the information transduction capacity of a gene can be tuned in *cis* and the amount of information transmitted increased by integrating the response of multiple genes. Nonetheless, for individual genes our results are consistent with the Msn2 pathway transmitting essentially error-free signal identity information, but unreliable signal intensity information, and therefore functioning more like a "noisy switch" than a "rheostat". Since many similar master regulators, such as p53, NF-κB, ERK and Hes1, also transduce information through regulation of signaling dynamics, it will be interesting to investigate whether dynamic cell signaling is generally limited to error-free transduction of only signal identity information.

MATERIALS AND METHODS

Microfluidics and time-lapse microscopy

Microscopy experiments were performed essentially as described previously (Hansen et al., 2015; Hansen and O'Shea, 2013). Briefly, yeast cells were grown overnight at 30°C with shaking at 180 RPM to an $OD_{600\ nm}$ of ca. 0.1 in low fluorescence medium, quickly collected by suction filtration, loaded into the five channels of a microfluidic device pretreated with concanavalin A and the setup mounted on a Zeiss AxioObserver Z1 inverted fluorescence microscope equipped with an Evolve EM-CCD camera (Photometrics), 63x oil-immersion objective (NA 1.4, Plan-Apochromat), Zeiss Colibri LEDs for excitation and an incubation chamber kept at 30°C. Solenoid valves programmed using custom-written software (MATLAB) control whether medium with or without 1-NM-PP1 is delivered to each microfluidic channel and the flow (ca. 1 μL/s) is driven by gravity. Control of 1-NM-PP1 delivery enables control of Msn2 pulsing (Figure 2) and a unique pulse sequence can be delivered to each of the five microfluidic channels. The microscope maintains focus and moves between each channel to acquire phase-contrast, YFP, CFP, RFP and iRFP images for 64 frames with a 2.5 min time resolution. For the amplitude modulation experiments, 1-NM-PP1 was added to each microfluidic channel for 70 min at the following concentrations: 100 nM, 175 nM, 275 nM, 413 nM, 690 nM, 1117 nM, 3 μM. For the frequency modulation experiments a concentration of 690 nM 1-NM-PP1 was used together with the following pulse sequences: one 5-min pulse; two 5-min pulses separated by a 40-min interval; three 5-min pulses separated by 25-min intervals; four 5-min pulses separated by 17.5-min intervals; five 5-min pulses separated by 13-min intervals; six 5-min pulses separated by 10-min intervals; seven 5-min pulses separated by 7.86-min intervals; eight 5-min pulses separated by 6.25-min intervals; nine 5-min pulses separated by 5-min intervals. Control software for the microfluidic device and a full protocol are provided elsewhere (Hansen et al., 2015). Image analysis was performed using custom-written software (MATLAB) that segments, tracks and quantifies single-cell time-traces and has been described previously (Hansen et al., 2015; Hansen and O'Shea, 2013). All raw single-cell data is available online as Supplementary File 1 and in (Hansen and O'Shea, 2015).

Computation of mutual information

The mutual information for a single reporter is defined in Equation 1 and the maximal mutual information given by:

$$I(R;S) = \max_{p(S)}\left[MI(R;S)\right] \quad \text{for} \quad \sum_i p(S_i) = 1; \quad p(S_i) \geq 0$$

The $p(S)$ that maximizes the mutual information is determined using the iterative Blahut-Arimoto algorithm. An unbiased I was estimated using jackknife sampling to correct for undersampling as has previously been described (Cheong et al., 2011; Slonim et al., 2005; Strong et al., 1998). The data were discretized by binning as shown in Figure 2. Maximal mutual information, I, and its error are reported as the mean and standard deviation, respectively, from calculating the unbiased I using 15 to 35 bins, inclusive.

To determine the maximal joint mutual information, I (Figure 4A), first consider the joint mutual information between the signal S and two responses R_1 (e.g. YFP) and R_2 (e.g. CFP):

$$MI(R_1, R_2; S) = MI(R_1; S) + MI(R_2; S|R_1)$$

Where $MI(R_1;S)$ is known from Equation 1 and $MI(R_2;S|R_1)$ is given by:

$$MI(R_2;S|R_1) = \sum_{i,j,k} p(R_1(i))p(R_2(j))p(S(k))\log_2\left(\frac{p(R_1(i))p(R_1(i),R_2(j),S(k))}{p(R_1(i))p(R_2(j))p(R_1(i),S(k))}\right)$$

The maximal joint mutual information is then given by:

$$I(R_1,R_2;S)=\max_{p(S)}\left[MI(R_1,R_2;S)\right] \quad \text{for} \quad \sum_i p(S_i)=1; \quad p(S_i)\geq 0$$

As before, $p(S)$ is obtained using the Blahut-Arimoto algorithm and the mean and error of I is obtained as for a single reporter, except using 8 to 20 bins, inclusive. Full details are given in Supplementary File 2.

Algorithm to estimate the intrinsic mutual information

Briefly, the total, intrinsic and extrinsic noise for each condition is calculated using dual-reporters (CFP/YFP) (Elowitz et al., 2002; Swain et al., 2002). The expression distributions in the absence of extrinsic noise are required to determine I_{int}. This is an intractable problem (Hilfinger and Paulsson, 2011). To estimate it, the raw, empirical YFP distribution is fitted to a gamma distribution ($\text{YFP}\sim\Gamma(a,b)$). Keeping the mean fixed, a new gamma distribution representing the YFP response in the absence of extrinsic noise is then inferred by filtering out the extrinsic contribution to the variance. This is repeated for each condition, each distribution is then discretized and the maximal mutual information, I, determined as above.

The accuracy of the algorithm was tested by simulating five linear and five non-linear stochastic gene expression models for both a fast and a slow promoter using the Gillespie algorithm under amplitude modulation (10 conditions). Extrinsic noise is added by picking the translation rate and TF concentration for each iteration from a gamma distribution. The algorithm was then applied to each data set with extrinsic noise and compared to simulation results with only intrinsic noise and the error calculated. In all 80 cases (10 models, 2 promoters, 4 levels of extrinsic noise), the error was less than 5% (in bits) and the mean error was less than 2%. Full details are given in Supplementary File 2.

Measurement noise, data processing and YFP quantification

Measurement noise is a major concern for information theoretical calculations and can lead to underestimates of mutual information. To control and minimize effects of noise, the following data processing pipeline was employed. For each single-cell, a time-trace of 64 YFP measurements is made (2.5 min interval). The fluorescence (in AU) is the mean pixel-intensity per cell corresponding to the YFP concentration. As can be seen in Figure 2 – figure supplement 1B and Figure 2 – figure supplement 2 from the single-cell YFP traces, YFP concentration generally reaches a plateau around or after the 100 min time-point (element 43 in the YFP vector). So the maximal YFP level in the cell is measured approximately 20 times before the experiment ends (element 64 in the YFP vector). Although there is slight noise in each measurement of the YFP concentration as shown in Figure 2 – figure supplement 2A (black circles), because YFP is independently measured ~20 times after it has reached a plateau, the actual YFP level can accurately be determined by smoothing (Figure 2 – figure supplement 2A, red line). The YFP trace is smoothed using an 11-point moving average filter and the vector is subsequently converted to a scalar by taking the maximal YFP value in the [33;64] range of elements. The scalar YFP concentration (Figure 2 – figure supplement 1B) is used for all information theoretical calculations. We believe that the protein concentration is the most biologically relevant measure of gene expression. For example, the activity of a stress response enzyme is generally determined by its concentration. But we note that had a different measure been used, e.g. had the dynamics of the YFP time-trace been included, different estimates of I would be obtained (see also Supplementary File 2 for a further discussion).

The following factors, among others, contribute to measurement noise: slight variations in microscope focusing; fluctuations in cellular autofluorescence; instrumentation variability (e.g. camera noise); day-to-day experimental variability; slight errors from automated image analysis.

Nonetheless, as is also evident from Figure 2 – figure supplement 2 measurement noise is small. For *HXK1* and *SIP18* I_{AM} and I_{FM} were independently measured twice in different strains: the *SIP18* dual-reporter strain (EY2813/ASH94), the *HXK1* dual-reporter strain (EY2810/ASH91) and the 1x reporter diploid (EY2972/ASH194). The results are shown in the table below:

I	*gene*::YFP / *gene*::CFP strain	1x *sip18* ::YFP / *hxk1* ::CFP strain
I_{AM}(*sip18*::YFP)	1.21 ± 0.03 bits	1.17 ± 0.02 bits
I_{FM}(*sip18*::YFP)	0.52 ± 0.06 bits	0.50 ± 0.05 bits
I_{AM}(*hxk1*::CFP/YFP)	1.30 ± 0.01 bits	1.30 ± 0.01 bits
I_{FM}(*hxk1*::CFP/YFP)	1.11 ± 0.01 bits	1.14 ± 0.01 bits

As is clear from the table above, the measurements of I_{AM} and I_{FM} between different strains (with slightly different genetic backgrounds) are highly similar and within error. This provides high confidence in the measurements and shows that the measurements are robust between different clones. Nonetheless, a constant noise source would cause all measurements to be underestimates by similar amounts. Therefore, the consistency of the measurements does not exclude the presence of a constant noise source. However, it is also important to note that most noise sources are "extrinsic" to the gene and will therefore partially be filtered out by the algorithm during the correction for extrinsic noise.

Strain construction

All strains used in this study are listed in Table 1. The diploid strains containing fluorescent reporters for the *SIP18* (ASH94/EY2813) and *HXK1* (ASH91/EY2810) promoters have been described previously (Hansen and O'Shea, 2013). These and all other *Saccharomyces cerevisiae* strains used in this study are from an *ADE*$^+$ strain in the W303 background (*MAT****a*** (EY0690) and *MAT****α*** (EY0691) *trp1 leu2 ura3 his3 can1 GAL*$^+$ *psi*$^+$). Standard methods for growing and genetically manipulating yeast was used throughout this study and all manipulations were performed in the same manner in both haploid mating types unless otherwise stated. Mating was performed by mixing haploids and selecting for diploids on SD –TRP –LEU plates. All genetic manipulations were verified by PCR.

To generate the *pSIP18* promoter mutants, the relevant segment of the promoter was replaced by *URA3* and followed by replacing the *URA3* fragment with a PCR generated fragment containing the relevant mutations and counterselection against *URA3*. The full sequence of the wild-type *SIP18* promoter and the mutant promoters are listed below.

> WT *SIP18* promoter

GCTCACTTTTTGTTGGTCTGTATTCATTCTGGATGTCTTGGTTGTAGAAATTTCTTTTATTGGTTCATTAAAGTCAAGGTAAATGGCGAGAACTAGAATAGAGT
TTTATTCTTTTTACCGTTATATAGATAATTCTAGCCGGGGGCGGTCG**CCCCT**GAGATTCCCGACATCAGTAAGACATAGTACTGTACGATTACTGTACGATTAA
TCTATCCACTTCAGATGTTCAACAATTCCTTTTGGCATTACGTATTAATACTTCATAGGATCGGCACCCTCCCTTAAGCCT**CCCCT**AAATGCTTTCGGTA**CCCC**
TTTAAGACAACTATCTCTTAACCTTCTGTATTTACTTGCATGTTACGTTGAGTCTCATTGGAGGTTTGCATCATATGTTTAGGTTTTTTTGGAAACGTGGACGG
CTCATAGTGATTGGTAAATGGGAGTTACGAATAAACGTATCTTAAAGGGAGCGGTATGTAAAATGGATAGATGATCATGAATACAGTACGAGGTGTAAAGAATG
ATGGGACTGAGAGGGCAATTATCATCCCTCAGAATCAACATCACAAACATATATAAAGCTCCCAATTCTGCCCCAAAGTTTTGTCCCTAGGCATTTTTAATCTT
TGTATCTGTGCTCTTTACTTTAGTAGAAAGGTATATAAAAAAGTATAGTCAAG

> *pSIP18* mut A promoter

GCTCACTTTTTGTTGGTCTGTATTCATTCTGGATGTCTTGGTTGTAGAAATTTCTTTTATTGGTTCATTAAAGTCAAGGTAAATGGCGAGAACTAGAATAGAGT
TTTATTCTTTTTACCGTTATATAGATAATTCTAGCCGGGGGCGGTCG**CCCCT**GAGATTCCCGACATCAGTAAGACATAGTACTGTACGATTACTGTACGATTAA
TCTATCCACTTCAGATGTTCAACAATTCCTTTTGGCATTACGTATTAATACTTCATAGGATCGGCACCCTCCCTTAAGCCT**~~CAACT~~**AAATGCTTTCGGTA**~~CAAC~~**
~~T~~TTAAGACAACTATCTCTTAACCTTCTGTATTTACTTGCATGTTACGTTGAGTCTCATTGGAGGTTTGCATCATATGTTTAGGTTTTTTTGGAAACGTGGACGG
CTCATAGTGATTGGTAAATGGGAGTTA**CCCCT**AAACGTATCTTAAAGGGA**CCCCT**ATGTAAAATGGATAG**CCCCT**CATGAATACAGTACGAGGTGTAAAGAATG
ATGGGACTGAGAGGGCAATTATCATCCCTCAGAATCAACATCACAAACATATATAAAGCTCCCAATTCTGCCCCAAAGTTTTGTCCCTAGGCATTTTTAATCTT
TGTATCTGTGCTCTTTACTTTAGTAGAAAGGTATATAAAAAAGTATAGTCAAG

> *pSIP18* mut B promoter

GCTCACTTTTTGTTGGTCTGTATTCATTCTGGATGTCTTGGTTGTAGAAATTTCTTTTATTGGTTCATTAAAGTCAAGGTAAATGGCGAGAACTAGAATAGAGT
TTTATTCTTTTTACCGTTATATAGATAATTCTAGCCGGGGGCGGTCG**CCCCT**GAGATTCCCGACATCAGTAAGACATAGTACTGTACGATTACTGTACGATTAA
TCTATCCACTTCAGATGTTCAACAATTCCTTTTGGCATTACGTATTAATACTTCATAGGATCGGCACCCTCCCTTAAGCCT**~~CAACT~~**AAATGCTTTCGGTA**~~CAAC~~**
~~T~~TTAAGACAACTATCTCTTAACCTTCTGTATTTACTTGCATGTTACGTTGAGTCTCATTGGAGGTTTGCATCATATGTTTAGGTTTTTTTGGAAACGTGGACGG
CTCATAGTGA**CCCCT**AAATGGGAGTTA**CCCCT**AAACGTATCTTAAAGGGA**CCCCT**ATGTAAAATGGATAG**CCCCT**CATGAATACAGTACGAGGTGTAAAGAATG
ATGGGACTGAGAGGGCAATTATCATCCCTCAGAATCAACATCACAAACATATATAAAGCTCCCAATTCTGCCCCAAAGTTTTGTCCCTAGGCATTTTTAATCTT
TGTATCTGTGCTCTTTACTTTAGTAGAAAGGTATATAAAAAAGTATAGTCAAG

To remove the Msn2 binding site (STRE 5'-CCCCT'-3'), the two central Cs were replaced by As (5'-CCCCT'-3' → 5'-CAACT'-3'), as shown in purple in the above sequences. The most upstream site in the *SIP18* promoter appears to be non-functional – deleting it has no effect on gene induction. Conversely, the two sites between -350 and -400 bp appear to be solely responsible for gene induction – deletion of both sites completely abolishes gene induction to below our detection limit. Mut A and Mut B have 3 and 4 new STRE sites, respectively, instead of the 2 STREs in the WT promoter. The position was chosen to be closer to the transcription start site, but in the largely nucleosome free region between two nucleosomes (Figure 2 – figure supplement 1C). The same manipulations were performed in both mating types and all microscopy experiments were conducted in diploid strains (Mut A: EY2969/ASH191; Mut B: EY2967/ASH189).

To generate the 1x and 2x reporter diploid strains (1x: EY2972/ASH194; 2x: EY2975/ASH197), strain EY2811/ASH92 (MAT**a** *sip18*::mCitrineV163A-HIS) and strain EY2809/ASH90 (MAT**α** *hxk1*::SCFP3A-HIS) were used as base strains. In EY2811, the *HXK1* ORF was replaced by *URA3* to generate EY2970/ASH192, which was used for the 1x reporter diploid, and *URA3* further replaced by a PCR fragment containing SCFP3A followed by the *ADH1* terminator and the *spHIS5* selection marker (from a pKT vector) using counterselection against *URA3*. This gave strain EY2973/ASH195, which was used for the 2x reporter diploid. Likewise, in EY2811 the *SIP18* ORF was replaced by *URA3* to generate EY2971/ASH193, which was used for the 1x reporter diploid, and *URA3* further replaced by a PCR fragment containing mCitrineV163A followed by the *ADH1* terminator and the *spHIS5* selection marker (from a pKT vector) using counterselection against *URA3*. This gave strain EY2974/ASH196, which was used for the 2x reporter diploid. Furthermore, the 1x reporter diploid (EY2972/ASH194) was generated by mating EY2970/ASH192 and EY2971/ASH193 and the 2x reporter diploid (EY2975/ASH197) generated by mating EY2973/ASH195 and EY2974/ASH196. In the 1x reporter diploid, no WT copies of the *SIP18* and *HXK1* genes are present to ensure that, in the case the encoded protein product could have an autoregulatory effect, this complication would be avoided.

Finally, we note that 1-NM-PP1 mediated gene induction of *HXK1* and *SIP18* is specific to Msn2. In an *msn2*Δ-deletion strain, neither *HXK1* nor *SIP18* are induced by 1-NM-PP1 (Hansen and O'Shea, 2013) and both promoters have been shown to directly bind Msn2 in ChIP experiments (Elfving et al., 2014; Huebert et al., 2012).

All strains are available upon request and all strains are derived from EY0690 and EY0691.

TABLE 1

Strain	Type	Strain details
EY0690	*MAT***a**	W303 (*trp1 leu2 ura3 his3 can1 GAL*$^+$ *psi*$^+$) (not generated in this study)
EY0691	*MAT***α**	W303 (*trp1 leu2 ura3 his3 can1 GAL*$^+$ *psi*$^+$) (not generated in this study)
EY2808/ ASH89	*MAT***a**	*TPK1*^{M164G} *TPK2*^{M147G} *TPK3*^{M165G} *msn4Δ::*TRP1 *MSN2*-mCherry *NHP6a*-iRFP::kanMX *hxk1::*mCitrine_V163A-spHIS5 (not generated in this study)
EY2809/ ASH90	*MAT***α**	*TPK1*^{M164G} *TPK2*^{M147G} *TPK3*^{M165G} *msn4Δ*::LEU2 *MSN2*-mCherry *NHP6a*-iRFP::kanMX *hxk1*::SCFP3A-spHIS5 (not generated in this study)
EY2810/ ASH91	Diploid	*TPK1*^{M164G} *TPK2*^{M147G} *TPK3*^{M165G} *msn4Δ::*TRP1/LEU2 *MSN2*-mCherry *NHP6a*-iRFP::kanMX *hxk1::*mCitrineV163A/SCFP3A-spHIS5 (not generated in this study)
EY2811/ ASH92	*MAT***a**	*TPK1*^{M164G} *TPK2*^{M147G} *TPK3*^{M165G} *msn4Δ::*TRP1 *MSN2*-mCherry *NHP6a*-iRFP::kanMX *sip18::*mCitrine_V163A-spHIS5 (not generated in this study)
EY2812/ ASH93	*MAT***α**	*TPK1*^{M164G} *TPK2*^{M147G} *TPK3*^{M165G} *msn4Δ*::LEU2 *MSN2*-mCherry *NHP6a*-iRFP::kanMX *sip18*::SCFP3A-spHIS5 (not generated in this study)
EY2813/ ASH94	Diploid	*TPK1*^{M164G} *TPK2*^{M147G} *TPK3*^{M165G} *msn4Δ::*TRP1/LEU2 *MSN2*-mCherry *NHP6a*-iRFP::kanMX *sip18::*mCitrineV163A/SCFP3A-spHIS5 (not generated in this study)
EY2964/ ASH139	*MAT* ***a***	*TPK1*^{M164G} *TPK2*^{M147G} *TPK3*^{M165G} *msn4Δ::*TRP1 *MSN2*-mCherry_DAD *NHP6a*-iRFP::kanMX *sip18*::mCitrine_V163A-HIS3 *pSIP18* Mut A 3 STREs
EY2965/ ASH140	*MAT* ***a***	*TPK1*^{M164G} *TPK2*^{M147G} *TPK3*^{M165G} *msn4Δ::*TRP1 *MSN2*-mCherry_DAD *NHP6a*-iRFP::kanMX *sip18*::mCitrine_V163A-HIS3 *pSIP18* Mut B 4 STREs
EY2966/ ASH188	*MAT***α**	*TPK1*^{M164G} *TPK2*^{M147G} *TPK3*^{M165G} *msn4Δ::LEU2 MSN2*-mCherry_DAD *NHP6a*-iRFP::kanMX *sip18::SCFP3A*-HIS3 *pSIP18* Mut B 4 STREs

EY2967/ ASH189	Diploid	*TPK1*^{M164G} *TPK2*^{M147G} *TPK3*^{M165G} *msn4Δ::*TRP1/LEU2 *MSN2*-mCherry_DAD *NHP6a*-iRFP::kanMX *sip18*::mCitrine_V163A/SCFP3A-HIS3 *pSIP18* Mut B 4 STREs
EY2968/ ASH190	*MAT***α**	*TPK1*^{M164G} *TPK2*^{M147G} *TPK3*^{M165G} *msn4Δ::LEU2 MSN2*-mCherry_DAD *NHP6a*-iRFP::kanMX *sip18::SCFP3A*-HIS3 *pSIP18* Mut A 3 STREs
EY2969/ ASH191	Diploid	*TPK1*^{M164G} *TPK2*^{M147G} *TPK3*^{M165G} *msn4Δ::*TRP1/LEU2 *MSN2*-mCherry_DAD *NHP6a*-iRFP::kanMX *sip18*::mCitrine_V163A/SCFP3A-HIS3 *pSIP18* Mut A 3 STREs
EY2970/ ASH192	*MAT* ***a***	*TPK1*^{M164G} *TPK2*^{M147G} *TPK3*^{M165G} *msn4Δ::*TRP1 *MSN2*-mCherry_DAD *NHP6a*-iRFP::kanMX *sip18*::mCitrine_V163A-HIS3 *hxk1*::URA3
EY2971/ ASH193	*MAT***α**	*TPK1*^{M164G} *TPK2*^{M147G} *TPK3*^{M165G} *msn4Δ*::LEU2 *MSN2*-mCherry_DAD *NHP6a*-iRFP::kanMX *hxk1*::SCFP3A_JCat-HIS3 *sip18*::URA3
EY2972/ ASH194	Diploid	*TPK1*^{M164G} *TPK2*^{M147G} *TPK3*^{M165G} *msn4Δ::*TRP1/LEU2 *MSN2*-mCherry_DAD *NHP6a*-iRFP::kanMX *sip18*::mCitrine_V163A-HIS3 *hxk1*::URA3 / *hxk1*::SCFP3A_JCat-HIS3 *sip18*::URA3 (1x reporter diploid)
EY2973/ ASH195	*MAT* ***a***	*TPK1*^{M164G} *TPK2*^{M147G} *TPK3*^{M165G} *msn4Δ::*TRP1 *MSN2*-mCherry_DAD *NHP6a*-iRFP::kanMX *sip18*::mCitrine_V163A-HIS3 *hxk1*::SCFP3A_JCat-HIS3
EY2974/ ASH196	*MAT***α**	*TPK1*^{M164G} *TPK2*^{M147G} *TPK3*^{M165G} *msn4Δ*::LEU2 *MSN2*-mCherry_DAD *NHP6a*-iRFP::kanMX *hxk1*::SCFP3A_JCat-HIS3 *sip18*::mCitrine_V163A-HIS3
EY2975/ ASH197	Diploid	*TPK1*^{M164G} *TPK2*^{M147G} *TPK3*^{M165G} *msn4Δ*::LEU2 *MSN2*-mCherry_DAD *NHP6a*-iRFP::kanMX **2x***hxk1*::SCFP3A_JCat-HIS3 **2x***sip18*::mCitrine_V163A-HIS3 (2x reporter diploid)

ADDITIONAL FILES

- Supplementary File 1. Raw single-cell time-trace data for *HXK1* (15259 cells), *SIP18* (21242 cells), *pSIP18* mut A (18203 cells), *pSIP18* mut B (17655 cells), 1x reporter diploid (21236 cells) and 2x reporter diploid (19222 cells). The data is also available from Dryad Digital Repository (Hansen and O'Shea, 2015).
- Supplementary File 2. Computation of Mutual Information. Complete description of information theoretical computations and the algorithm.
- Figure 2 – figure supplement 1. How time-lapse data is converted to histograms and promoter maps and noise data.
- Figure 2 – figure supplement 2. Data processing and control of measurement noise.
- Figure 3 – figure supplement 1. Input noise and variability in Msn2 abundance.
- Figure 4 – figure supplement 1. Summary of results for 1x reporter diploid.
- Figure 4 – figure supplement 2. Summary of results for 2x reporter diploid.

ACKNOWLEDGEMENTS

We thank Raymond Cheong, Gašper Tkačik and Mikhail Tikhonov for insightful discussions. We thank Nan Hao, Dann Huh, Arvind Subramaniam, Matthew Brennan, Roshni Wadhwani, Andrian Gutu, Shankar Mukherji, Kapil Amarnath, Bodo Stern, Sharad Ramanathan and members of the O'Shea lab for discussions and critically reading the manuscript. This work was performed in part at the Center for Nanoscale Systems at Harvard University, a member of the National Nanotechnology Infrastructure Network (NNIN), which is supported by the National Science Foundation under NSF award no. ECS-0335765. Image analysis and model simulations were run on the Odyssey cluster supported by the FAS Division of Science, Research Computing Group at Harvard University. The Howard Hughes Medical Institute supported this work.

COMPETING INTERESTS

EKO: Chief Scientific Officer and a Vice President at the Howard Hughes Medical Institute, one of the three founding funders of *eLife*. ASH: no competing interests.

FIGURE AND VIDEO LEGENDS

Figure 1

Encoding and transmitting signal identity and intensity information in the dynamics of a single TF.

(**A**) Different signals (e.g. stress or ligand exposure) can be encoded in the dynamics of a single TF. Signal identity is encoded in the type of TF dynamics: a sustained pulse (signal A) or nuclear pulsing (signal B). Signal intensity (e.g. ligand concentration) is encoded in the amplitude for signal A, but in the frequency for signal B. Different dynamical patterns of TF activation can activate distinct, but specific, downstream gene expression programs.

(**B**) Applying an information theoretic framework to cell signaling, a gene promoter can be considered a channel. A graded population-level dose-response belies the complexity of the single-cell response: it shows the mean expression at points a, b, c and d, but not the width or variance of their distributions.

(**C**) Two extreme models. In the "rheostat model", signal intensity information encoded in the frequency or amplitude of a TF leads to non-overlapping gene expression distributions (a, b, c and d). Thus, by reading the gene expression output the cell can accurately determine the input signal intensity and high information transmission is achieved. Conversely, in the "noisy switch model", as a consequence of overlapping gene expression distributions (a, b, c and d) information about signal intensity is permanently lost: the cell can distinguish ON/OFF (signal identity), but the expression of a target gene cannot be fine-tuned to the stress intensity.

Figure 2

Information transduction by promoters with respect to amplitude and frequency modulation.

(**A**) Cells containing either the *hxk1*::YFP or *sip18*::YFP reporter were exposed to either no activation or a 70-min pulse of seven increasing amplitudes from ca. 25% (100 nM 1-NM-PP1) to 100% (3 μM 1-NM-PP1) of maximal Msn2-mCherry nuclear localization and single-cell gene expression monitored. For each single-cell time-trace, YFP concentration is converted to a scalar by taking the maximal YFP value after smoothing. For each Msn2-mCherry input (a fit to the raw data is shown on the left (AM: Msn2 input)), the gene expression distribution is plotted as a histogram of the same color on the right for *HXK1* and *SIP18*. The population-averaged dose-response (top) is obtained by calculating the YFP histogram mean for each Msn2 input condition.

(**B**) Cells containing either the *hxk1*::YFP or *sip18*::YFP reporter were exposed to either no activation or from one to nine 5-min pulses of Msn2-mCherry nuclear localization (ca. 75% of maximal nuclear Msn2-mCherry, 690 nM 1-NM-PP1) at increasing frequency. All calculations were performed as in (**A**).

(**C**) Cells containing either the *pSIP18* mut A::YFP reporter or the *pSIP18* mut B::YFP reporter were exposed to amplitude modulation as in (**A**).

(**D**) Cells containing either the *pSIP18* mut A::YFP reporter or the *pSIP18* mut B::YFP reporter were exposed to frequency modulation as in (**B**).

Mutual information, *I*, and its error are calculated as described in Supplementary File 2. Full details on data processing are given in Materials and Methods. Each plot of an Msn2 input pulse and YFP expression is based on data from ca. 1000 cells from at least three replicates.

All raw single-cell time-lapse microscopy source data for *HXK1* (15259 cells), *SIP18* (21242 cells), *pSIP18* mut A (18203 cells) and *pSIP18* mut B (17655 cells) for this figure is available online as Supplementary File 1 and in (Hansen and O'Shea, 2015).

The following figure supplements are available for Figure 2:

Figure-figure supplement 1. How time-lapse data is converted to histograms, promoter maps and noise data.

Figure-figure supplement 2. Data processing and control of measurement noise.

Figure 3

An algorithm for estimating intrinsic mutual information.

(**A**) Genetically identical cells can have shifted single-cell dose-responses due to gene-extrinsic effects such as variation in Msn2 abundance and cell cycle phase. Measuring the response of a single reporter (YFP)

642 therefore underestimates mutual information. By introducing an additional reporter (CFP), we can
643 distinguish extrinsic noise such as a shifted dose-response since this affects both CFP and YFP equally,
644 from true intrinsic stochasticity.
645 (**B**) Overview of algorithm. By fitting a gamma distribution to the raw YFP data, calculating the CFP/YFP
646 covariance and filtering this component out of the total variance, an intrinsic YFP distribution can be
647 estimated (left). By repeating this for each dose-response distribution, intrinsic mutual information can be
648 estimated (right). Full details on the algorithm are given in Supplementary File 2.
649 (**C**) By applying the algorithm to the data from Figure 2 (solid bars), we can estimate intrinsic mutual
650 information (hatched bars).
651 The following figure supplements are available for Figure 3:
652 **Figure-figure supplement 1**. Input noise and variability in Msn2 abundance.
653
654
655 **Figure 4**
656 Integrating the response of more than one gene improves information transmission.
657 (**A**) The AM and FM experiments (Figure 2) were repeated for diploid strains containing either one copy
658 (1x) of the *hxk1*::CFP and *sip18*::YFP reporters or two copies (2x) of the *hxk1*::CFP and *sip18*::YFP
659 reporters and individual and joint mutual information determined (full details on calculations are given in
660 Supplementary File 2).
661 (**B**) 2x *sip18*::YFP vs. 2x *hxk1*::CFP scatterplot showing expression for three experiments: no input (light
662 purple), five 5-min pulses of 690 nM 1-NM-PP1 separated by 13-min intervals (orange) or one 70-min pulse
663 of 3 μM 1-NM-PP1 (green). For each condition, 600 cells are shown. The YFP/CFP expression is the
664 maximal value after each time-trace has reached a plateau. The inset shows a zoom-in highlighting the 'no
665 input' condition.
666 All raw single-cell time-lapse microscopy source data for the 1x reporter diploid (21236 cells) and 2x
667 reporter diploid (19222 cells) for this figure is available online as Supplementary File 1 and in (Hansen and
668 O'Shea, 2015).
669 The following figure supplements are available for Figure 4:
670 **Figure-figure supplement 1**. Summary of results for 1x reporter diploid.
671 **Figure-figure supplement 2**. Summary of results for 2x reporter diploid.
672
673 **Video 1**
674 A typical experiment. Mut B cells were grown in a microfluidic device and exposed to six 5-min Msn2 pulses
675 separated by 10 min and phase contrast (top left), Msn2-mCherry (top right), CFP (bottom left) and YFP
676 (bottom right) reporter expression monitored. Video 1 consists of 64 frames at 2.5 min resolution and
677 images have been compressed, cropped and contrast adjusted, but not corrected for photobleaching.
678
679

FIGURE LEGENDS FOR FIGURE SUPPLEMENTS

Figure 2 – Figure supplement 1. How time-lapse data is converted to histograms and promoter maps and noise data.

(**A**) Overview of strains. To visualize and quantify the subcellular localization of Msn2 it was C-terminally tagged with the red fluorescent protein mCherry. A nuclear protein, NHP6a, was C-terminally tagged with iRFP, an infrared fluorescent protein (Filonov et al., 2011; Hansen and O'Shea, 2013), to visualize the nucleus for segmentation purposes. All three catalytic subunits of PKA were mutated to contain an analogue-sensitive M→G mutation (*TPK1*^{M164G} *TPK2*^{M147G} *TPK3*^{M165G}). These mutations render all three PKA subunits sensitive to the small molecule 1-NM-PP1 (Bishop et al., 2000; Hao and O'Shea, 2012; Zaman et al., 2009). Thus, when 1-NM-PP1 is added, PKA is inhibited, Msn2-mCherry is no longer phosphorylated by PKA, gets dephosphorylated, and translocates into the nucleus where it can bind to and activate target genes. To visualize gene expression, the ORFs of target genes were replaced with YFP (mCitrineV163A) and CFP (SCFP3A) on homologues chromosomes in diploid cells, as has been described previously (Hansen et al., 2015; Hansen and O'Shea, 2013; Kremers et al., 2006). The inhibitor, 1-NM-PP1 is shown on the right and its synthesis has been described previously (Hansen and O'Shea, 2013).

(**B**) An illustration of how the YFP histograms are obtained for each condition. For a specific amplitude or frequency (not shown), the response of ~1000 cells is measured (only ~300 cells shown here for ease of visualization). For each single cell time-trace a moving average smoothing filter is applied to remove any technical noise and the maximal YFP value is determined after the trace has reached a plateau. This is repeated for all single cells and a YFP histogram is generated by binning. The procedure is then repeated for all the Msn2 conditions (e.g. the no input and all the AM conditions) to generate a full single-cell dose-response (right). This data is then used to calculate the maximal mutual information with respect to amplitude modulation, I_{AM}.

(**C**) Promoter nucleosome occupancy maps. The upstream promoter region (-800 to 0 bp from ATG site) is shown for each promoter. Msn2 binding sites (STRE 5'-CCCCT-3') are shown in red triangles and nucleosome occupancy data (grey) is from (Hansen and O'Shea, 2013). The *SIP18* promoter has three Msn2 binding sites. The most upstream site is seemingly non-functional – removing it does not affect gene induction. The two sites (close to -400 bp) are required – removing these two sites abolishes gene induction. *pSIP18* mut A and mut B have three and four new binding sites, respectively, in between the two nucleosomes close to the transcription start site.

(**D**) Dynamic range and noise. Removing the two WT Msn2 binding sites and replacing them with three or four binding sites, respectively, substantially increases the dynamic range (defined as the response to a 70 min pulse at 3 μM 1-NM-PP1).

How the total (red), intrinsic (blue) and extrinsic (green) noise scales with the Msn2 amplitude (for a 70 min pulse; top) or the frequency (at 690 nM 1-NM-PP1; bottom) for all four promoters is shown. The y-axis scale is different in each case.

Figure 2 – Figure supplement 2. Data processing and control of measurement noise.

(**A**) Data processing illustration. Controlling measurement noise is important, because high measurement noise will cause measurements of mutual information to be underestimates. To minimize effects of measurement noise coming e.g. from improper focusing by the microscope, autofluorescence and camera noise, slight errors in cell segmentation and other sources, multiple YFP measurements are made. For each single cell, the YFP level is measured 64 times at 2.5 min time resolution. In general, measurement noise is modest at very low YFP expression – in part due to cellular autofluorescence – but negligible at high YFP expression.As an example of very low YFP expression, a single cell time trace is shown on the left (*SIP18*, 70 min, 100 nM 1-NM-PP1). By smoothing the raw YFP data (black circles), an accurate estimation of the YFP level can be obtained (red line). As an example of very high YFP expression, a raw and smoothed single cell time trace is shown on the right (mut B, 70 min, 3 μM 1-NM-PP1).

(**B**) Example of raw data at very low YFP expression (*SIP18*, 70 min, 100 nM 1-NM-PP1). Raw YFP time-traces of 100 randomly chosen single cells are shown on the left and the same YFP time-traces, after

smoothing as illustrated in **A)**, are shown on the right. Although the raw YFP data suffers from modest measurement noise, the actual YFP level can be accurately estimated by smoothing.
(**C**) Example of raw data at low YFP expression (mut A, 70 min, 100 nM 1-NM-PP1). Raw YFP time-traces of 100 randomly chosen single cells are shown on the left and the same YFP time-traces, after smoothing as illustrated in **A)**, are shown on the right.
(**D**) Example of raw data at high YFP expression (mut B, 70 min, 3 μM 1-NM-PP1). Raw YFP time-traces of 100 randomly chosen single cells are shown on the left and the same YFP time-traces, after smoothing as illustrated in **A)**, are shown on the right.
Furthermore, all raw single-cell time-trace data for *HXK1* (15259 cells), *SIP18* (21242 cells), *pSIP18* mut A (18203 cells), *pSIP18* mut B (17655 cells), 1x reporter diploid (21236 cells) and 2x reporter diploid (19222 cells) is available as Supplementary File 1 and in (Hansen and O'Shea, 2015).

Figure 3 – Figure supplement 1. Input noise and variability in Msn2 abundance.
(**A**) Variability in Msn2 abundance. One source of noise in our system is non-genetic cell-to-cell variability in Msn2 abundance. Msn2 is a low-abundance protein: there are only a few hundred molecules in each cell (Ghaemmaghami et al., 2003). Therefore, precisely measuring Msn2 abundance is challenging. Furthermore, the nucleus moves in and out of focus during time-lapse acquisition. To estimate the variation in Msn2 abundance, cells (*pSIP18* mut B) were grown in the microfluidic device and exposed to a 70-min pulse of either 0, 100 nM, 175 nM, 275 nM, 413 nM, 690 nM, 1117 nM or 3 μM 1-NM-PP1. Msn2-mCherry nuclear localization was measured using a 5-frame z-stack series of 0, ± 1.2 μm, ± 2.4 μm above and below the focal plane using a 500 ms exposure time and imaging every 10 min. Msn2-mCherry fluorescence was corrected for photobleaching. We collected two frames before and after 1-NM-PP1 exposure to calculate the baseline level of Msn2 before 1-NM-PP1 treatment. In **A)**, we show the mean and standard deviation for each timepoint for each concentration.
(**B**) To calculate mutual information between 1-NM-PP1 input and Msn2-mCherry dynamics, we use the data from **A)** and calculate I_{AM}(1-NM-PP1; Msn2) = 2.06 ± 0.03 bits. We quantify Msn2-mCherry localization in absolute units as the mean nuclear Msn2 level across the seven measurements while Msn2 is nuclear – this also corresponds to the total time-integrated nuclear level of Msn2 (Msn2 'Area Under the Curve' or AUC). In total, we measured 2996 single cells. Using Msn2 variability in response to 3 μM 1-NM-PP1, we estimate the cell-to-cell variability of Msn2 to be CV~15%. However, given measurement noise we stress that CV~15% and I~2.06 bits are likely over- and underestimates, respectively. Note that Msn2 is a low abundance protein (Ghaemmaghami et al., 2003). Previous proteomic studies showed that essentially no yeast proteins have CV<10% (Newman et al., 2006). Therefore, Msn2 is among the least variable low abundance proteins in yeast.
(**C**) This figure is plotted using data from Figure 2 for *HXK1* (Hansen and O'Shea, 2015). In red is shown the input and in black are shown traces from 10 representative single cells. We did not do a finely spaced z-stack series for this experiment, which is necessary to accurately quantify the concentration of Msn2 in the nucleus – this causes too much photobleaching to be compatible with imaging at reasonable temporal resolution (2.5 min here). Nonetheless, as can be seen, the black traces faithfully track the input with limited noise. For each cell plotted above, we also measured *hxk1*::CFP and *hxk1*::YFP gene expression.
(**D**) To accurately quantify Msn2-mCherry dynamics during FM input, we acquired a finely spaced z-stack series at high time-resolution (1 min). This causes too high photobleaching to be compatible with sustained time-lapse imaging. Therefore, we are only able to collect data at this resolution for a single 5-min pulse. The mean (black dots) and standard deviation (error bars) for 132 single cells (*pSIP18* mut B) is shown. As can be seen, Msn2-mCherry accurately tracks the microfluidic 1-NM-PP1 input with limited noise also during FM input. In a population of cells, Msn2 translocates to the nucleus in every single cell during 1-NM-PP1 exposure.
(**F**) To calculate mutual information between 1-NM-PP1 input and Msn2-mCherry dynamics, we use the data from **D)** and estimate I_{FM}(1-NM-PP1; Msn2) = 2.23 ± 0.03 bits. Given measurement noise, this is likely an underestimate. We quantify Msn2-mCherry localization in absolute units as the total nuclear Msn2 level across the ten measurements while Msn2 is nuclear (five during the pulse, five after the pulse) – this also

corresponds to the total time-integrated nuclear level of Msn2 (Msn2 'Area Under the Curve' or AUC). With data from **D)**, we measure the distribution of cell-to-cell variability for a single 5-min pulse. To calculate I_{FM}, we then extrapolate by multiplying the AUC probability distribution by the pulse number of each experiment since Msn2 tracks the 1-NM-PP1 input as faithfully for the first pulse as for the subsequent pulses. Ideally, one would measure the Msn2 AUC at 1-min time resolution and with finely spaced z-stacks throughout the entire time-lapse experiment, but this is not technically possible due to photobleaching.

Figure 4 – Figure supplement 1. Summary of results for 1x reporter diploid.

This figure shows single and joint distribution histograms for the 1x reporter diploid (*sip18*::YFP *hxk1*::CFP).

Top panel, left: Cells containing both the *sip18*::YFP and *hxk1*::CFP reporters were exposed to either no activation or a 70-min pulse of seven increasing amplitudes from ca. 25% (100 nM 1-NM-PP1) to 100% (3 μM 1-NM-PP1) of maximal Msn2-mCherry nuclear localization and single-cell gene expression was monitored. For each single-cell time-trace, YFP expression is converted to a scalar by taking the maximal YFP value after smoothing. For each Msn2-mCherry input (a fit to the raw data is shown on the left (AM: Msn2 input)), the gene expression distribution is plotted as a histogram of the same color on the right for *HXK1* and *SIP18*. The population-averaged dose-response (top) is obtained by calculating the YFP histogram mean for each Msn2 input condition.

Top panel, right: Cells containing both the *sip18*::YFP and *hxk1*::CFP reporters were exposed to either no activation or from one to nine 5-min pulses of Msn2-mCherry nuclear localization (ca. 75% of maximal nuclear Msn2-mCherry, 690 nM 1-NM-PP1) at increasing frequency. All calculations were performed as described above.

Middle panel: The discretized joint AM distribution is shown with *sip18*::YFP on the y-axis and *hxk1*::CFP on the x-axis. The color of each bin corresponds to the probability – dark blue means unoccupied and red corresponds to the highest probability. The single-cell time-traces were converted to scalars as illustrated in Figure 2 – figure supplement 1B. Each individual subplot corresponds to a different condition (Msn2 amplitude) and the data has been binned such that the low expression bins are much smaller and therefore harder to see on the plot.

Bottom panel: Same as for the joint AM distribution in the middle panel except for the joint FM distribution. Each subplot now corresponds to a specific frequency (and thus number of pulses).

Figure 4 – Figure supplement 2. Summary of results for 2x reporter diploid.

This figure shows single and joint distribution histograms for the 2x reporter diploid (2x *sip18*::YFP 2x *hxk1*::CFP).

Top panel, left: Cells containing both the 2x *sip18*::YFP and 2x *hxk1*::CFP reporters were exposed to either no activation or a 70-min pulse of seven increasing amplitudes from ca. 25% (100 nM 1-NM-PP1) to 100% (3 μM 1-NM-PP1) of maximal Msn2-mCherry nuclear localization and single-cell gene expression monitored. For each single-cell time-trace, YFP expression is converted to a scalar by taking the maximal YFP value after smoothing. For each Msn2-mCherry input (a fit to the raw data is shown on the left (AM: Msn2 input)), the gene expression distribution is plotted as a histogram of the same color on the right for *HXK1* and *SIP18*. The population-averaged dose-response (top) is obtained by calculating the YFP histogram mean for each Msn2 input condition.

Top panel, right: Cells containing both the 2x *sip18*::YFP and 2x *hxk1*::CFP reporters were exposed to either no activation or from one to nine 5-min pulses of Msn2-mCherry nuclear localization (ca. 75% of maximal nuclear Msn2-mCherry, 690 nM 1-NM-PP1) at increasing frequency. All calculations were performed as described above.

Middle panel: The discretized joint AM distribution is shown with 2x *sip18*::YFP on the y-axis and 2x *hxk1*::CFP on the x-axis. The color of each bin corresponds to the probability – dark blue means unoccupied and red corresponds to the highest probability. The single-cell time-traces were converted to scalars as illustrated in Figure 2 – figure supplement 1B. Each individual subplot corresponds to a different condition (Msn2 amplitude) and the data has been binned such that the low expression bins are much smaller and therefore harder to see on the plot.

Bottom panel: Same as for the joint AM distribution except for the joint FM distribution. Each subplot now corresponds to a specific frequency (and thus number of pulses).

REFERENCES

Albeck, J.G., Mills, G.B., and Brugge, J.S. (2013). Frequency-modulated pulses of ERK activity transmit quantitative proliferation signals. Mol Cell *49*, 249-261.

Aoki, K., Kamioka, Y., and Matsuda, M. (2013). Fluorescence resonance energy transfer imaging of cell signaling from in vitro to in vivo: basis of biosensor construction, live imaging, and image processing. Dev Growth Differ *55*, 515-522.

Balaban, N.Q., Merrin, J., Chait, R., Kowalik, L., and Leibler, S. (2004). Bacterial persistence as a phenotypic switch. Science *305*, 1622-1625.

Bar-Even, A., Paulsson, J., Maheshri, N., Carmi, M., O'Shea, E., Pilpel, Y., and Barkai, N. (2006). Noise in protein expression scales with natural protein abundance. Nat Genet *38*, 636-643.

Batchelor, E., Loewer, A., Mock, C., and Lahav, G. (2011). Stimulus-dependent dynamics of p53 in single cells. Mol Syst Biol *7*.

Behar, M., Dohlman, H.G., and Elston, T.C. (2007). Kinetic insulation as an effective mechanism for achieving pathway specificity in intracellular signaling networks. P Natl Acad Sci USA *104*, 16146-16151.

Behar, M., and Hoffmann, A. (2010). Understanding the temporal codes of intra-cellular signals. Curr Opin Genet Dev *20*, 684-693.

Berridge, M.J., Lipp, P., and Bootman, M.D. (2000). The versatility and universality of calcium signalling. Nat Rev Mol Cell Biol *1*, 11-21.

Bishop, A.C., Ubersax, J.A., Petsch, D.T., Matheos, D.P., Gray, N.S., Blethrow, J., Shimizu, E., Tsien, J.Z., Schultz, P.G., Rose, M.D*., et al.* (2000). A chemical switch for inhibitor-sensitive alleles of any protein kinase. Nature *407*, 395-401.

Blake, W.J., Balazsi, G., Kohanski, M.A., Isaacs, F.J., Murphy, K.F., Kuang, Y., Cantor, C.R., Walt, D.R., and Collins, J.J. (2006). Phenotypic consequences of promoter-mediated transcriptional noise. Mol Cell *24*, 853-865.

Bowsher, C.G., and Swain, P.S. (2012). Identifying sources of variation and the flow of information in biochemical networks. P Natl Acad Sci USA *109*, E1320-E1328.

Bowsher, C.G., and Swain, P.S. (2014). Environmental sensing, information transfer, and cellular decision-making. Curr Opin Biotech *28*, 149-155.

Cai, L., Dalal, C.K., and Elowitz, M.B. (2008). Frequency-modulated nuclear localization bursts coordinate gene regulation. Nature *455*, 485-490.

Cheong, R., Rhee, A., Wang, C.J., Nemenman, I., and Levchenko, A. (2011). Information transduction capacity of noisy biochemical signaling networks. Science *334*, 354-358.

Coulon, A., Chow, C.C., Singer, R.H., and Larson, D.R. (2013). Eukaryotic transcriptional dynamics: from single molecules to cell populations. Nature reviews Genetics *14*, 572-584.

Cover, T.M., and Thomas, J.A. (2006). Elements of information theory, 2nd edn (Hoboken, N.J., Wiley-Interscience).

Csete, M., and Doyle, J. (2004). Bow ties, metabolism and disease. Trends Biotechnol *22*, 446-450.

Dalal, C.K., Cai, L., Lin, Y.H., Rahbar, K., and Elowitz, M.B. (2014). Pulsatile Dynamics in the Yeast Proteome. Current Biology *24*, 2189-2194.

de Nadal, E., Ammerer, G., and Posas, F. (2011). Controlling gene expression in response to stress. Nature reviews Genetics *12*, 833-845.

de Ronde, W., and ten Wolde, P.R. (2014). Multiplexing oscillatory biochemical signals. Phys Biol *11*.

de Ronde, W., Tostevin, F., and ten Wolde, P.R. (2011). Multiplexing biochemical signals. Phys Rev Lett *107*, 048101.

Dubuis, J.O., Tkacik, G., Wieschaus, E.F., Gregor, T., and Bialek, W. (2013). Positional information, in bits. P Natl Acad Sci USA *110*, 16301-16308.

Elfving, N., Chereji, R.V., Bharatula, V., Bjorklund, S., Morozov, A.V., and Broach, J.R. (2014). A dynamic interplay of nucleosome and Msn2 binding regulates kinetics of gene activation and repression following stress. Nucleic Acids Res *42*, 5468-5482.

Elowitz, M.B., Levine, A.J., Siggia, E.D., and Swain, P.S. (2002). Stochastic gene expression in a single cell. Science *297*, 1183-1186.

Ferrell, J.E., Jr., and Machleder, E.M. (1998). The biochemical basis of an all-or-none cell fate switch in Xenopus oocytes. Science *280*, 895-898.

Filonov, G.S., Piatkevich, K.D., Ting, L.M., Zhang, J.H., Kim, K., and Verkhusha, V.V. (2011). Bright and stable near-infrared fluorescent protein for in vivo imaging. Nat Biotechnol *29*, 757-U133.

Ghaemmaghami, S., Huh, W., Bower, K., Howson, R.W., Belle, A., Dephoure, N., O'Shea, E.K., and Weissman, J.S. (2003). Global analysis of protein expression in yeast. Nature *425*, 737-741.

Gregor, T., Tank, D.W., Wieschaus, E.F., and Bialek, W. (2007). Probing the limits to positional information. Cell *130*, 153-164.

Hansen, A.S., Hao, N., and O'Shea, E.K. (2015). High-throughput microfluidics to control and measure signaling dynamics in single yeast cells. under review.
Hansen, A.S., and O'Shea, E.K. (2013). Promoter decoding of transcription factor dynamics involves a trade-off between noise and control of gene expression. Mol Syst Biol *9*.
Hansen, A.S., and O'Shea, E.K. (2015). Data from: Limits on information transduction through regulation of signaling dynamics. Dryad Digital Repository.
Hao, N., Budnik, B.A., Gunawardena, J., and O'Shea, E.K. (2013). Tunable Signal Processing Through Modular Control of Transcription Factor Translocation. Science *339*, 460-464.
Hao, N., and O'Shea, E.K. (2012). Signal-dependent dynamics of transcription factor translocation controls gene expression. Nat Struct Mol Biol *19*, 31-U47.
Harima, Y., Imayoshi, I., Shimojo, H., Kobayashi, T., and Kageyama, R. (2014). The roles and mechanism of ultradian oscillatory expression of the mouse Hes genes. Semin Cell Dev Biol *34*, 85-90.
Herrero, P., Galindez, J., Ruiz, N., Martinezcampa, C., and Moreno, F. (1995). Transcriptional Regulation of the Saccharomyces-Cerevisiae Hxk1, Hxk2 and Glk1 Genes. Yeast *11*, 137-144.
Hilfinger, A., and Paulsson, J. (2011). Separating intrinsic from extrinsic fluctuations in dynamic biological systems. P Natl Acad Sci USA *108*, 12167-12172.
Huebert, D.J., Kuan, P.F., Keles, S., and Gasch, A.P. (2012). Dynamic Changes in Nucleosome Occupancy Are Not Predictive of Gene Expression Dynamics but Are Linked to Transcription and Chromatin Regulators. Mol Cell Biol *32*, 1645-1653.
Imayoshi, I., Isomura, A., Harima, Y., Kawaguchi, K., Kori, H., Miyachi, H., Fujiwara, T., Ishidate, F., and Kageyama, R. (2013). Oscillatory Control of Factors Determining Multipotency and Fate in Mouse Neural Progenitors. Science *342*, 1203-1208.
Jacquet, M., Renault, G., Lallet, S., De Mey, J., and Goldbeter, A. (2003). Oscillatory nucleocytoplasmic shuttling of the general stress response transcriptional activators Msn2 and Msn4 in Saccharomyces cerevisiae. The Journal of cell biology *161*, 497-505.
Kremers, G.J., Goedhart, J., van Munster, E.B., and Gadella, T.W.J. (2006). Cyan and yellow super fluorescent proteins with improved brightness, protein folding, and FRET Forster radius. Biochemistry-Us *45*, 6570-6580.
Lahav, G., Rosenfeld, N., Sigal, A., Geva-Zatorsky, N., Levine, A.J., Elowitz, M.B., and Alon, U. (2004). Dynamics of the p53-Mdm2 feedback loop in individual cells. Nat Genet *36*, 147-150.
Lempiainen, H., and Shore, D. (2009). Growth control and ribosome biogenesis. Curr Opin Cell Biol *21*, 855-863.
Lestas, I., Vinnicombe, G., and Paulsson, J. (2010). Fundamental limits on the suppression of molecular fluctuations. Nature *467*, 174-178.
Levchenko, A., and Nemenman, I. (2014). Cellular noise and information transmission. Curr Opin Biotech *28*, 156-164.
Levine, J.H., Lin, Y.H., and Elowitz, M.B. (2013). Functional Roles of Pulsing in Genetic Circuits. Science *342*, 1193-1200.
Li, Y., and Goldbeter, A. (1989). Frequency specificity in intercellular communication. Influence of patterns of periodic signaling on target cell responsiveness. Biophys J *55*, 125-145.
Mc Mahon, S.S., Sim, A., Filippi, S., Johnson, R., Liepe, J., Smith, D., and Stumpf, M.P. (2014). Information theory and signal transduction systems: From molecular information processing to network inference. Semin Cell Dev Biol *35C*, 98-108.
Mehta, P., Goyal, S., Long, T., Bassler, B.L., and Wingreen, N.S. (2009). Information processing and signal integration in bacterial quorum sensing. Mol Syst Biol *5*, 325.
Nemenman, I. (2012). Information theory and adaptation. In Quantitative Biology: From Molecular to Cellular Systems, M.E. Wall, ed. (CRC Press).
Newman, J.R.S., Ghaemmaghami, S., Ihmels, J., Breslow, D.K., Noble, M., DeRisi, J.L., and Weissman, J.S. (2006). Single-cell proteomic analysis of S-cerevisiae reveals the architecture of biological noise. Nature *441*, 840-846.
Petrenko, N., Chereji, R.V., McClean, M.N., Morozov, A.V., and Broach, J.R. (2013). Noise and interlocking signaling pathways promote distinct transcription factor dynamics in response to different stresses. Mol Biol Cell *24*, 2045-2057.
Purvis, J.E., and Lahav, G. (2013). Encoding and Decoding Cellular Information through Signaling Dynamics. Cell *152*, 945-956.
Rapp, P.E., Mees, A.I., and Sparrow, C.T. (1981). Frequency encoded biochemical regulation is more accurate than amplitude dependent control. J Theor Biol *90*, 531-544.
Rhee, A., Cheong, R., and Levchenko, A. (2012). The application of information theory to biochemical signaling systems. Phys Biol *9*, 045011.

Rieckh, G., and Tkacik, G. (2014). Noise and information transmission in promoters with multiple internal States. Biophys J *106*, 1194-1204.
Rodriguez-Porrata, B., Carmona-Gutierrez, D., Reisenbichler, A., Bauer, M., Lopez, G., Escote, X., Mas, A., Madeo, F., and Cordero-Otero, R. (2012). Sip18 hydrophilin prevents yeast cell death during desiccation stress. J Appl Microbiol *112*, 512-525.
Sanchez, A., and Golding, I. (2013). Genetic determinants and cellular constraints in noisy gene expression. Science *342*, 1188-1193.
Selimkhanov, J., Taylor, B., Yao, J., Pilko, A., Albeck, J., Hoffmann, A., Tsimring, L., and Wollman, R. (2014). Accurate information transmission through dynamic biochemical signaling networks. Science *346*, 1370-1373.
Shannon, C.E. (1948). A Mathematical Theory of Communication. At&T Tech J *27*, 623-656.
Skerker, J.M., Perchuk, B.S., Siryaporn, A., Lubin, E.A., Ashenberg, O., Goulian, M., and Laub, M.T. (2008). Rewiring the specificity of two-component signal transduction systems. Cell *133*, 1043-1054.
Slonim, N., Atwal, G.S., Tkacik, G., and Bialek, W. (2005). Information-based clustering. P Natl Acad Sci USA *102*, 18297-18302.
Strong, S.P., Koberle, R., van Steveninck, R.R.D., and Bialek, W. (1998). Entropy and information in neural spike trains. Phys Rev Lett *80*, 197-200.
Swain, P.S., Elowitz, M.B., and Siggia, E.D. (2002). Intrinsic and extrinsic contributions to stochasticity in gene expression. P Natl Acad Sci USA *99*, 12795-12800.
Tkacik, G., Callan, C.G., Jr., and Bialek, W. (2008). Information flow and optimization in transcriptional regulation. P Natl Acad Sci USA *105*, 12265-12270.
Tkacik, G., and Walczak, A.M. (2011). Information transmission in genetic regulatory networks: a review. J Phys Condens Matter *23*, 153102.
Tkacik, G., Walczak, A.M., and Bialek, W. (2009). Optimizing information flow in small genetic networks. Phys Rev E *80*.
Toettcher, J.E., Weiner, O.D., and Lim, W.A. (2013). Using optogenetics to interrogate the dynamic control of signal transmission by the Ras/Erk module. Cell *155*, 1422-1434.
Tostevin, F., and ten Wolde, P.R. (2009). Mutual information between input and output trajectories of biochemical networks. Phys Rev Lett *102*, 218101.
Tostevin, F., ten Wolde, P.R., and Howard, M. (2007). Fundamental limits to position determination by concentration gradients. PLoS Comput Biol *3*, e78.
Uda, S., Saito, T.H., Kudo, T., Kokaji, T., Tsuchiya, T., Kubota, H., Komori, Y., Ozaki, Y., and Kuroda, S. (2013). Robustness and compensation of information transmission of signaling pathways. Science *341*, 558-561.
Voliotis, M., Perrett, R.M., McWilliams, C., McArdle, C.A., and Bowsher, C.G. (2014). Information transfer by leaky, heterogeneous, protein kinase signaling systems. P Natl Acad Sci USA *111*, E326-333.
Waltermann, C., and Klipp, E. (2011). Information theory based approaches to cellular signaling. Biochim Biophys Acta *1810*, 924-932.
Warmflash, A., Zhang, Q.X., Sorre, B., Vonica, A., Siggia, E.D., and Brivanlou, A.H. (2012). Dynamics of TGF-beta signaling reveal adaptive and pulsatile behaviors reflected in the nuclear localization of transcription factor Smad4. P Natl Acad Sci USA *109*, E1947-E1956.
Werner, S.L., Barken, D., and Hoffmann, A. (2005). Stimulus specificity of gene expression programs determined by temporal control of IKK activity. Science *309*, 1857-1861.
Yosef, N., and Regev, A. (2011). Impulse Control: Temporal Dynamics in Gene Transcription. Cell *144*, 886-896.
Zaman, S., Lippman, S.I., Schneper, L., Slonim, N., and Broach, J.R. (2009). Glucose regulates transcription in yeast through a network of signaling pathways. Mol Syst Biol *5*.
Ziv, E., Nemenman, I., and Wiggins, C.H. (2007). Optimal signal processing in small stochastic biochemical networks. Plos One *2*, e1077.
Zopf, C.J., Quinn, K., Zeidman, J., and Maheshri, N. (2013). Cell-Cycle Dependence of Transcription Dominates Noise in Gene Expression. PLoS Comput Biol *9*.

Figure 1

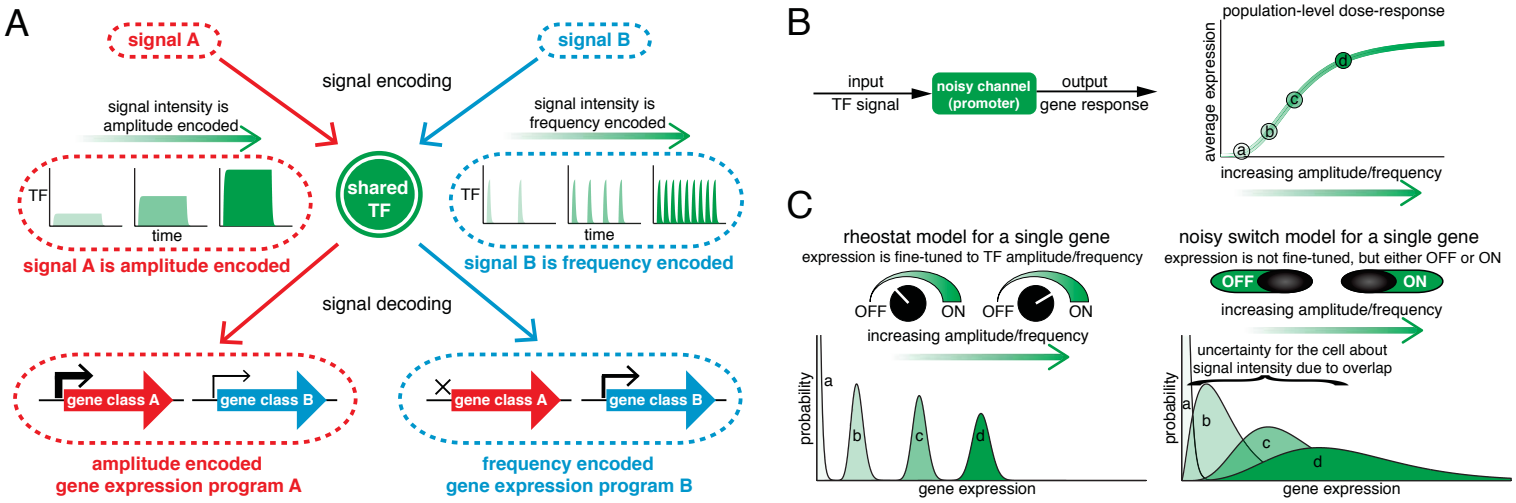
A
signal A
signal B
signal encoding
signal intensity is amplitude encoded
signal intensity is frequency encoded
shared TF
TF
time
TF
time
signal A is amplitude encoded
signal B is frequency encoded
signal decoding
gene class A
gene class B
gene class A
gene class B
amplitude encoded gene expression program A
frequency encoded gene expression program B
B
input TF signal
noisy channel (promoter)
output gene response
population-level dose-response
average expression
a
b
c
d
increasing amplitude/frequency
C
rheostat model for a single gene
expression is fine-tuned to TF amplitude/frequency
OFF
ON
OFF
ON
increasing amplitude/frequency
probability
a
b
c
d
gene expression
noisy switch model for a single gene
expression is not fine-tuned, but either OFF or ON
OFF
ON
increasing amplitude/frequency
uncertainty for the cell about signal intensity due to overlap
probability
a
b
c
d
gene expression

Figure 2

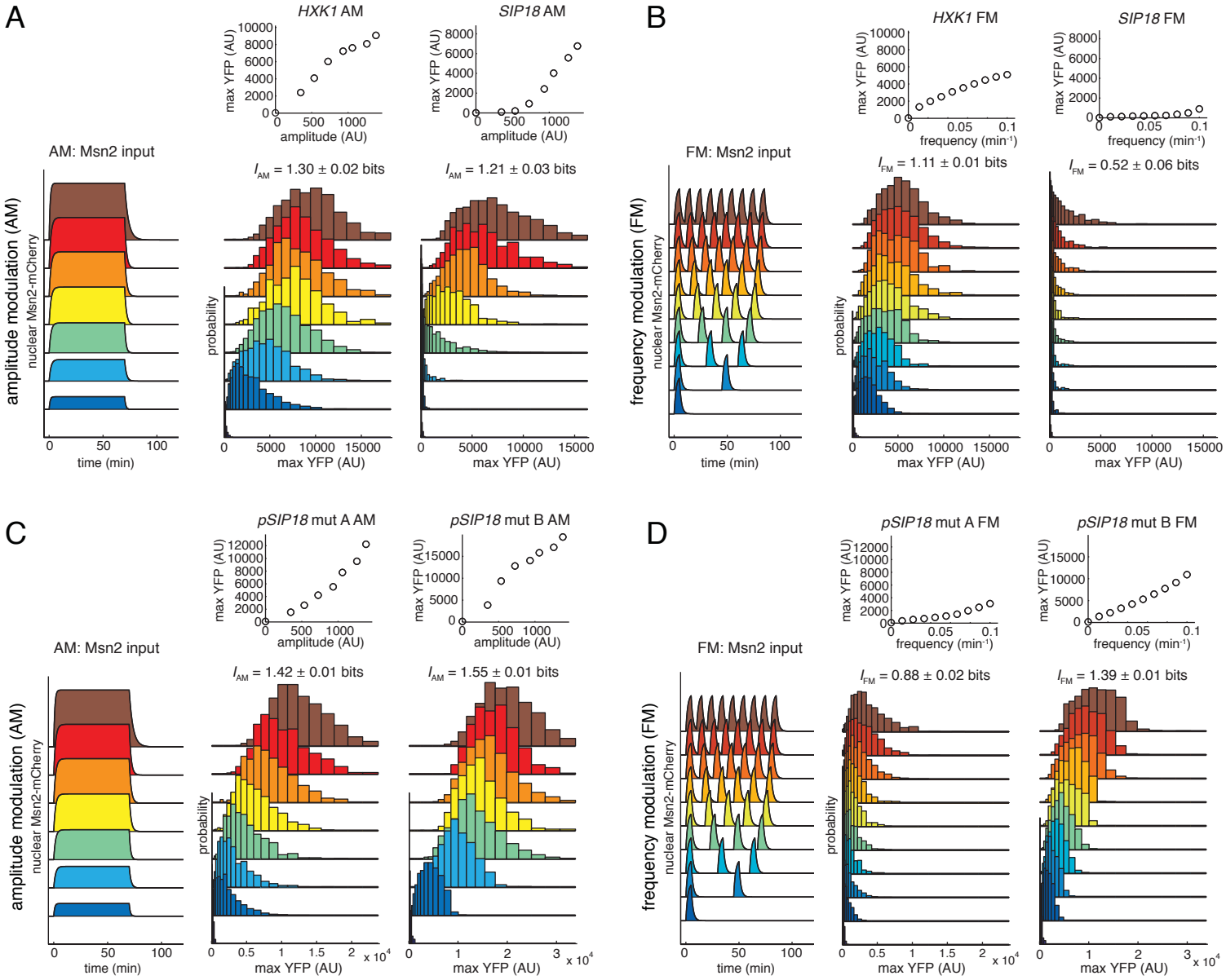
A
HXK1 AM
SIP18 AM
max YFP (AU)
amplitude (AU)
AM: Msn2 input
I_AM = 1.30 ± 0.02 bits
I_AM = 1.21 ± 0.03 bits
amplitude modulation (AM)
nuclear Msn2-mCherry
probability
time (min)
max YFP (AU)
B
HXK1 FM
SIP18 FM
frequency (min-1)
FM: Msn2 input
I_FM = 1.11 ± 0.01 bits
I_FM = 0.52 ± 0.06 bits
frequency modulation (FM)
C
pSIP18 mut A AM
pSIP18 mut B AM
I_AM = 1.42 ± 0.01 bits
I_AM = 1.55 ± 0.01 bits
D
pSIP18 mut A FM
pSIP18 mut B FM
I_FM = 0.88 ± 0.02 bits
I_FM = 1.39 ± 0.01 bits

Figure 3

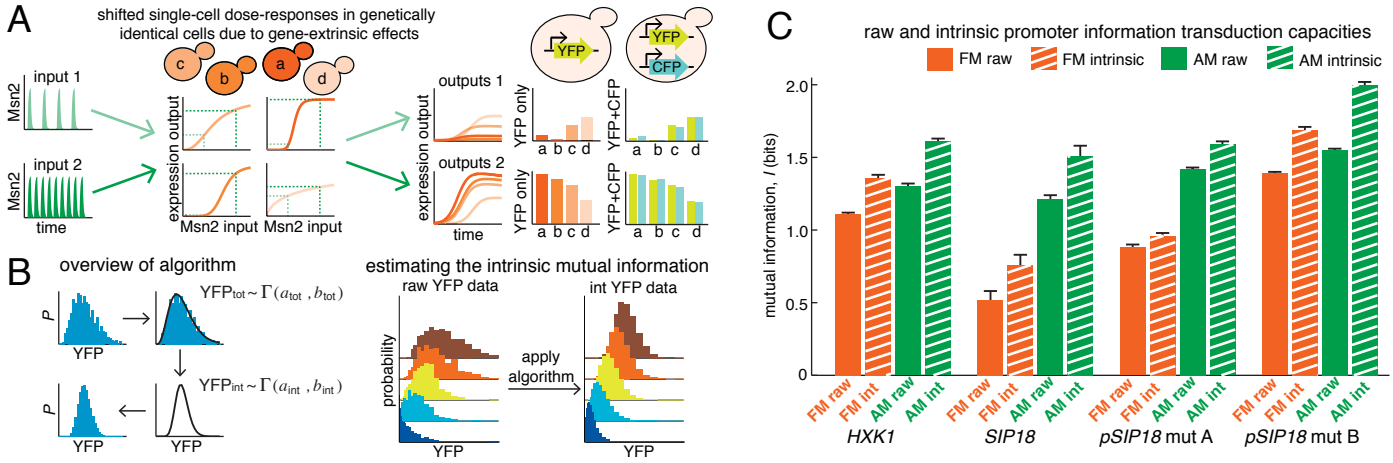
A
shifted single-cell dose-responses in genetically identical cells due to gene-extrinsic effects
input 1
input 2
Msn2
time
expression output
Msn2 input
outputs 1
outputs 2
YFP only
YFP+CFP
a b c d
YFP
CFP
B
overview of algorithm
$YFP_{tot} \sim \Gamma(a_{tot}, b_{tot})$
$YFP_{int} \sim \Gamma(a_{int}, b_{int})$
P
estimating the intrinsic mutual information
raw YFP data
int YFP data
probability
apply algorithm
C
raw and intrinsic promoter information transduction capacities
FM raw
FM intrinsic
AM raw
AM intrinsic
mutual information, I (bits)
HXK1
SIP18
pSIP18 mut A
pSIP18 mut B

Figure 4

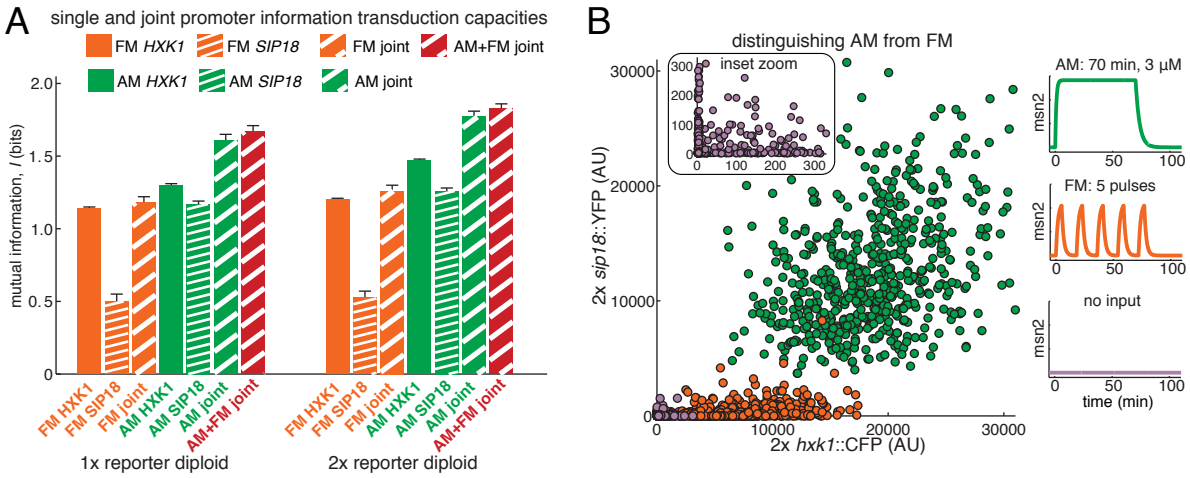
A
single and joint promoter information transduction capacities
FM HXK1
FM SIP18
FM joint
AM+FM joint
AM HXK1
AM SIP18
AM joint
mutual information, I (bits)
2.0
1.5
1.0
0.5
0
FM HXK1
FM SIP18
FM joint
AM HXK1
AM SIP18
AM joint
AM+FM joint
1x reporter diploid
2x reporter diploid
B
distinguishing AM from FM
inset zoom
2x sip18::YFP (AU)
2x hxk1::CFP (AU)
30000
20000
10000
0
AM: 70 min, 3 μM
FM: 5 pulses
no input
msn2
time (min)